Enhanced phase and charge diffusion due to radio-frequency/microwave excitation in Bloch transistors

Saxon Liou and Watson Kuo

Citation: AIP Advances **3**, 082127 (2013); doi: 10.1063/1.4819486
View online: http://dx.doi.org/10.1063/1.4819486
View Table of Contents: http://aipadvances.aip.org/resource/1/AAIDBI/v3/i8
Published by the AIP Publishing LLC.

AIP ADVANCES **3**, 082127 (2013)

Enhanced phase and charge diffusion due to radio-frequency/microwave excitation in Bloch transistors

Saxon Liou[1,3] and Watson Kuo[1,2,a]
[1]*Department of Physics, National Chung Hsing University, Taichung 402, Taiwan*
[2]*Center of Nanoscience and Nanotechnology, and Institute of Nanoscience, National Chung Hsing University, Taichung 402, Taiwan*
[3]*Institute of Physics, Academia Sinica, Taipei 115, Taiwan*

(Received 22 May 2013; accepted 12 August 2013; published online 22 August 2013)

Current-voltage characteristics and switching current of Bloch transistors under radio-frequency/microwave excitations were experimental studied, respectively revealing pronounced summational superconducting phase diffusion and central-island charge diffusion. The phase diffusion, which can be quantified by the zero-bias resistance, was found minimal when two charge states in the transistor are degenerate. The switching current, which also reflects the charge diffusion, was observed that becomes minimal at the degeneracy beyond a threshold in ac driving power. The charge diffusion was analyzed using an electric dipolar interaction between the photon field and excess charge on the central island. [http://dx.doi.org/10.1063/1.4819486]

I. INTRODUCTION

A Bloch transistor (BT) is two mesoscopic Josephson junctions separated by a small superconducting central island. It holds superconducting phase coherency, which is governed by the gauge invariant superconducting phases of the two consisting junctions, ϕ_1 and ϕ_2. Because of the small capacitance of the central island, a BT may exhibit robust single charge effect and a gate voltage V_g can modulate the Cooper-pair transport.[1] The two effects yield a symmetric BT the following hamiltonian, $H_B = 4E_C(n - n_g)^2 + E_J \cos(\theta/2)\cos\phi$, in which E_C and E_J are charging energy and Josephson energy of the central island of the transistor.[2] As quantum conjugate quantities, n and $\phi = (\phi_1 - \phi_2)/2$ respectively denote the number of excess Cooper-pairs(CPs) and superconducting phase on the island. Gate charge number $n_g = C_g V_g/2e$ represents the effect of V_g electrostatically coupled via a gate capacitance C_g. $\theta = \phi_1 + \phi_2$ denotes the summational (or total) phase difference across the source and drain junctions. In general, the significance of phase coherency and charging effect depends on the ratio E_J/E_C[3] and dissipation[4–6].

The BT is of great interest since it exhibits phase-charge self-duality.[7] One of the most interesting consequences of duality is the case of the junction system irradiated by radio-frequency/microwave (RF/MW).[8] Phase coherent junction systems under ac driving have been studied by using current-voltage (*IV*) characteristic measurement. These works conclude that when the ac frequency is high, there would be phase mode-locking phenomenon yielding voltage steps,[9] whereas at rather low frequencies, there is enhanced phase diffusion.[10] One the other hand, the current steps induced by mode-locking and charge diffusion of an underdamped single junction can be expected.[8] Such an experiment can be carried out on a Josephson junction coupled to an electromagnetic environment of extremely high impedance.[11]

For BTs, combined Josephson coherency and charging effects are more easily to observe. Indeed, previous works successfully explained the observed voltage steps in *IV* curves using mode-locking

[a]Corresponding author email: wkuo@phys.nchu.edu.tw

of the summational phase θ.[12,13] On the other hand, in a charge-dominant junction systems, the ac driving of a frequency of ω may result in a charge pumping behavior, $I = q\omega/2\pi$. q is e for electron while $2e$ for CP pumping.[14,15] However, IV measurements do not provide the information of central island quantum state: CP number n and the differential phase ϕ, which should not be overlooked. To observe the n, people have been applied different method such as charge detection by a single electron transistor[16–18] or monitoring the current through a dissipative probe.[19] On the other hand, to observed ϕ, one may consider the supercurrent, I_s of the Bloch transistor from the phase-current relationship:

$$I_s = \frac{2e}{\hbar}\left\langle \frac{\partial H_B}{\partial \theta} \right\rangle = \frac{eE_J}{\hbar}\left\langle \cos\phi \sin\frac{\theta}{2} \right\rangle. \quad (1)$$

Here $\langle \cdots \rangle$ denote the ensemble average. The switching current I_{sw} is the maximal supercurrent a BT can sustain before it switches from the zero-voltage state to the finite-voltage state and becomes $I_{sw} = eE_J\langle\cos\phi\rangle/\hbar$ when θ is treated as a classical variable. By noting that the operator $\cos\phi = \sum_n (|n+1\rangle\langle n| + |n-1\rangle\langle n|)/2$, one can calculate the expectation value by solving the ground state in the representation of charge basis, $|n\rangle$. For the transistor exhibiting phase dominant behavior, one can experimentally observe a clearly switching current in the vicinity of zero bias voltage modulated by the gate-voltage.[20–22] In particular I_{sw} as a function of gate charge exhibits the so-called "Coulomb oscillation".

In this paper, we present experimental results on the BT under RF/MW excitation. Especially we focus on the V_g-dependent switching current, which give us information of the dynamics of n and ϕ. The experimental results uncovered two significant forms of electromagnetic wave coupling based on distinct RF/MW polarizations. For the central-island quantities, the device geometry prefers an interaction between electromagnetic waves and the electric dipole produced by excess charges on the island. Such a model predicts enhanced charge diffusion so as to bring in the inversion of Coulomb oscillation.

II. EXPERIMENTAL METHODS

For our experiment, BTs were fabricated by electron-beam lithography and standard shadow evaporation of aluminum on silicon substrates with a Si_3N_4 or SiO_2 insulating layer. $Al/AlO_x/Al$ tunnel junctions were formed using in-situ oxidation of deposited aluminum leads under 3×10^{-2} torr oxygen pressure for 3 minutes. Because of their small charging energies, the devices were cooled in a dilution refrigerator to a base temperature of 30 mK for measurement. For registration of their switching current I_{sw}, the transistor was biased by a current source, which was periodically ramped upward to cause a switching from the zero-voltage state to the finite voltage state. The switching event was determined when the device voltage exceeded a threshold of about 50 μV. Once the switching occurred, the bias-current was logged using a sample-and-hold circuit, and further digitized by a multi-meter. Two versions of experimental setup were used for introducing the RF/MW excitation in our work: For BT-1 and BT-2, a current loop antenna, which generated an ac magnetic dipole moment. BT-3 was imbedded in a LC resonator—as the setup of a RF single electron transistor.[23] The antenna setup allowed us a study for a broadband excitation, while the resonator setup was strict to a small frequency range near the resonance. The excitation RF/MW frequency ranged from 0.1 GHz to 20 GHz in our work.

III. EXPERIMENTAL RESULTS

A. Phase coherent and charging behaviors

As revealed by scanning electron microscopy images, Fig. 1(a), the Josephson junctions had a typical junction area of about 100 nm $\times$ 100 nm, yielding a central island charging energy $E_C = 80$ μeV. According to previous works, the normal state resistance of the tunnel junction, R_N, strongly affects the Cooper-pair tunneling so as to control the quantum fluctuation of superconducting phase in the transistors. Hence devices with different R_N were selected for a comparison. Table I lists

TABLE I. Important parameters of the Bloch transistors. (note that R_N is for single junction.)

Device	R_N (kΩ)	E_J (μeV)	E_C (μeV)	Δ_{sc} (μeV)	G_0 ($n_g = 0$)(μS)	I_{sw} ($n_g = 0$)(nA)
BT-1	13.1	105	~80	210	2.8	0.05
BT-2	7.7	177	~80	210	165	1.58
BT-3	12	92	~80	170	8.2	0.42

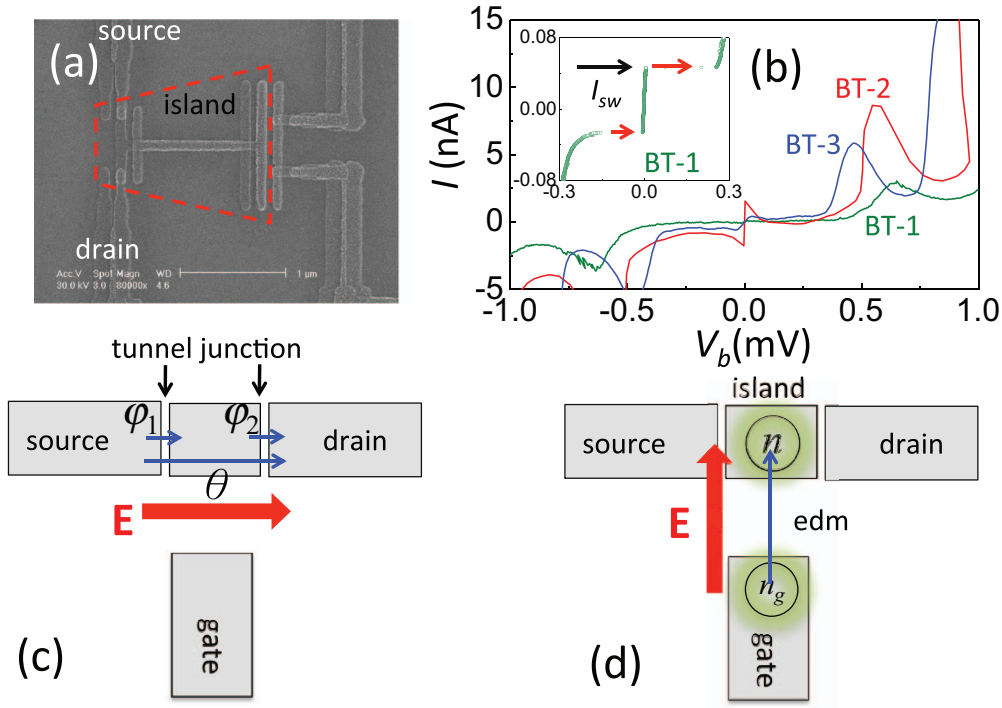

FIG. 1. (a) The scanning electron micrograph of a Bloch transistor, whose central island is marked by the dotted box. (b) The current-voltage characteristics of Bloch transistors under study. One can clear distinguish the coherent supercurrent in the vicinity of zero bias voltage and Josephson-quasi-particle current peak at 0.5 mV. The transistor with a lower R_N exhibits a larger supercurrent. Inset shows the switching current of BT-1 of about 60 nA. Two ways a BT affected by the ac driving: (c) The BT can be coupled to external ac field **E** via the summational phase difference $\theta = \phi_1 + \phi_2$, giving a phase diffusion behavior. (d) The BT can be coupled to external ac field via a electric dipole moment (edm) induced by excess CP number n.

important parameters of 3 devices under study. For example, BT-1 has a (central island) Josephson coupling energy of 105 μeV according to Ambegoakar-Baratoff relation, $E_J = \Delta_{SC} R_Q / R_N$ with $R_N = 13.1$ kΩ. Here the superconducting gap, Δ_{SC} of our thermal-evaporated aluminum was about 210 μeV (or 170 μeV for BT-3) while $R_Q = h/4e^2 = 6.5$ kΩ, is the quantum resistance for Cooper-pairs. We note that the E_C values are always over-estimated under robust charge fluctuation when $R_N \sim R_Q$. At the base temperature, the *IV* curve demonstrated robust coherent Cooper-pair tunneling features, such as supercurrent and Josephson quasi-particle current inside the superconducting gap (namely, when bias voltage $V_b < 4\Delta_{SC}$). Because of the hysteresis nature of the Josephson junctions, by current-biasing the transistor and ramping upward the current, we could observe a switching from the zero-voltage state to the finite voltage state at the switching current, I_{sw}. In general, the higher E_J value, the larger I_{sw} and the smaller zero-bias conductance, G_0.

As shown in Fig. 2(a), the histogram of I_{sw} of BT-1 at various V_g exhibited an oscillatory behavior—the Coulomb oscillation—in absence of microwave excitation (MW off). The average I_{sw} would follow the $\langle \cos \phi \rangle$ function calculated by using an E_J/E_C value of 2 as marked by the solid curves. Although higher than the value using the E_C derived from a geometric junction capacitance, this E_J/E_C value remains reasonable because of the quantum fluctuations in low resistance junctions.

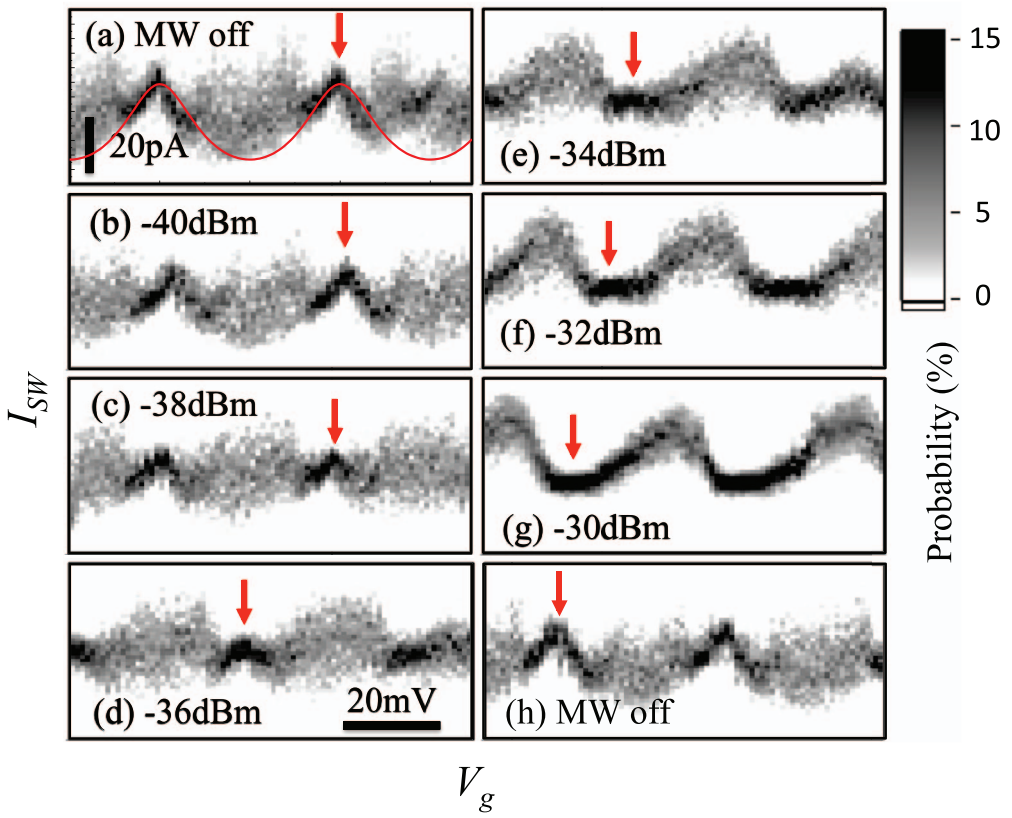

FIG. 2. Family of the intensity plots for switching current histogram for BT-1 under the 18 GHz MW driving at various driving powers. Each histogram contains 200 repeating I_{sw} measurement results. When ac driving is absent (a)(h), the switching current will be maximal at n_g is half-integers. The "width" of switching current distribution allow us to identify the drift of offset charge. The red arrows indicate the gate voltages corresponding to a minimal fluctuation in I_{sw}. When the MW power exceeds −36 dBm, the switching current becomes minimal at V_g of minimal I_{sw} fluctuation, yielding an inverted Coulomb oscillation.

We note that the fluctuation of I_{sw} (or the width of distribution) was minimal when I_{sw} was maximal. This may be due to thermal effect or remaining high-frequency noise from the electromagnetic environment. Because the V_g tunes the energy degeneracy of two lowest charge states, the fluctuation is also periodic in V_g.

Fig. 2(b)–2(g) show the histogram of I_{sw} when the devices driven by 18 GHz MW at elevated MW powers, P_{ac}. It is worthy to note that such a high frequency driving only affect I_{sw} but not the zero-bias conductance, G_0. A lower frequency RF would reduce G_0, turning the IV curve into a blockade structure at a certain power level. In this case, the measurement of I_{sw} became ambiguous. We will come back to this point later. By identifying the V_g value (as marked by red arrows) corresponding to the minimal I_{sw} fluctuation, we obtained two major findings: (1) the microwave introduced an effective (dc) gate charge offset. (2) the Coulomb oscillation of I_{sw} got inverted at $P_{ac} = -34$ dBm if the drift of charge offset was casted aside. The microwave-induced charge offset was history-dependent, as one can be compare in Fig. 2(a) and Fig. 2(h), which shows the Coulomb oscillation after the microwave was turned off (MW off). Being intriguing and unexpected, the inversion of Coulomb oscillation deserved a carefully analysis.

B. Phase diffusion due to ac driving

Here we will focus on the case that the RF/MW frequency ω is low, namely $\hbar\omega < k_B T \ll \hbar\omega_p$. The BTs under the driving of higher frequency produces clear Shapiro steps in the IV curves and have been reported earlier.[13] In the low frequency regime, we can neglect the photon absorption

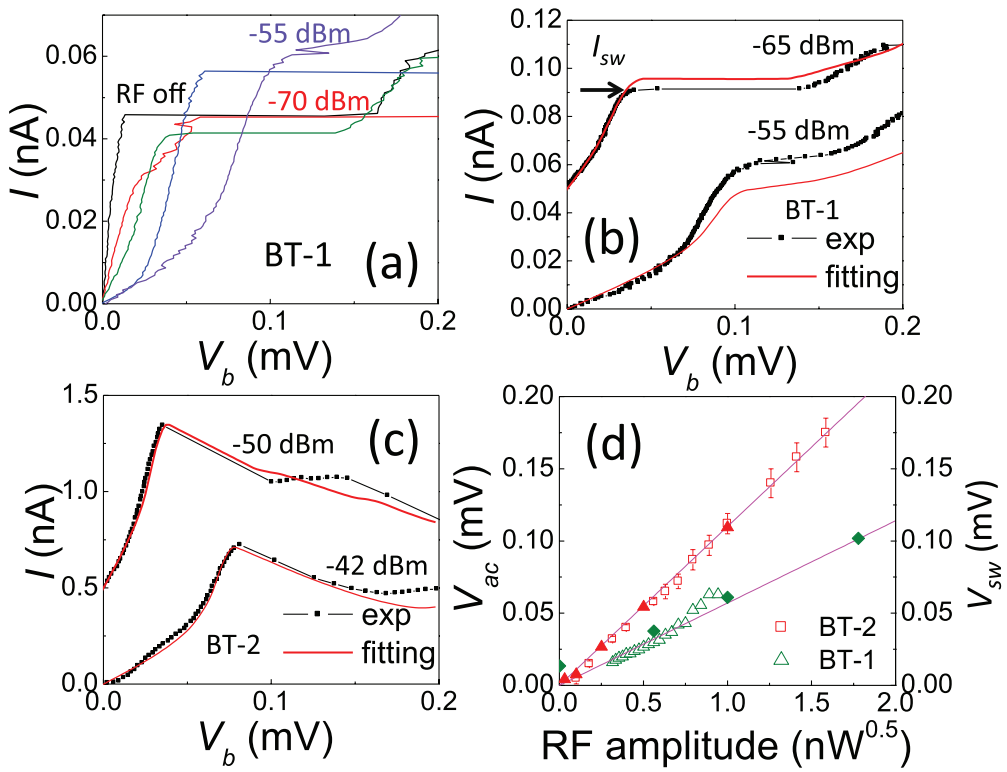

FIG. 3. (a) The current-voltage characteristic in the vicinity of zero bias voltage when BT-1 is excited by 1.6 GHz RF at elevated RF powers (5 dBm per step). The gate charge $n_g = 0.5$. As the power increases, the transistor evolves from a superconductor-like to a blockaded *IV*. (b) The experimental (red) and calculated (black) *IV* characteristic excited by 1.6 GHz at $P_{ac} = -65$ dBm and -55 dBm. The calculation is a fit to Eq. (2) based on the coupling model shown in Fig. 1(c). At $P_{ac} = -55$ dBm, the calculated result slightly deviates from the experimental one because the model predicts a smaller I_{sw}. (c) The experimental and calculated *IV* curves for BT-2 under 0.94 GHz RF excitation. The phase diffusion model agrees better because the robust phase coherency in BT-2. (d) The fitting parameter V_{ac} for BT-1 (△) and BT-2 (□), and the switching voltage V_{sw} for BT-1 (▲) and BT-2 (■). Both V_{ac} and V_{sw} show a linear dependence of RF amplitude. Here the RF amplitude for BT-2 data is scaled by a factor of 10.

process and treat the excitation as an ac driving force for the summational phase θ to yield $\dot{\phi}_1 \simeq \dot{\phi}_2 = \dot{\theta}/2 = eV_{ac}/\hbar$. V_{ac} represents the effective ac voltage across the transistor and is proportional to $\sqrt{P_{ac}}$. Such model as depicted in Fig. 1(c) schematically, has been considered before.[10,24] By calculating the phase correlation function, $\langle e^{i\theta(t)} e^{-i\theta(0)} \rangle$ due to phase diffusion by ac excitation, one obtains the spectral function

$$P(E) = \sum_{n=-\infty}^{\infty} J_n^2 \left(\frac{2eV_{ac}}{\hbar\omega} \right) P_0 (E - n\hbar\omega).$$

Here P_0 is the spectral function in absence of RF/MW. The spectral function gives an incoherent Cooper-pair tunneling that

$$I(V_b) = \sum_{n=-\infty}^{\infty} J_n^2 \left(\frac{2eV_{ac}}{\hbar\omega} \right) I^0 \left(V_b - \frac{n\hbar\omega}{2e} \right) = \frac{1}{2\pi} \int_0^{2\pi} I^0 (V_b + V_{ac} \cos u)\, du, \tag{2}$$

in which V_b is the dc voltage across the transistor and $I^0(V_b)$ is the device current as a function of V_b in absence of ac excitation.

Fig. 3(a) illustrates a family of *IV* characteristics of BT-1 under 1.6 GHz RF driving at various power at $n_g = 0.5$, a condition for minimal phase fluctuation. The zero-bias resistance gradually gets larger and larger, and the *IV* curve evolves into a blockade-like curve. Although under such a strong RF excitation, the phase coherency could sustain and the transistor exhibited switching at a finite dc

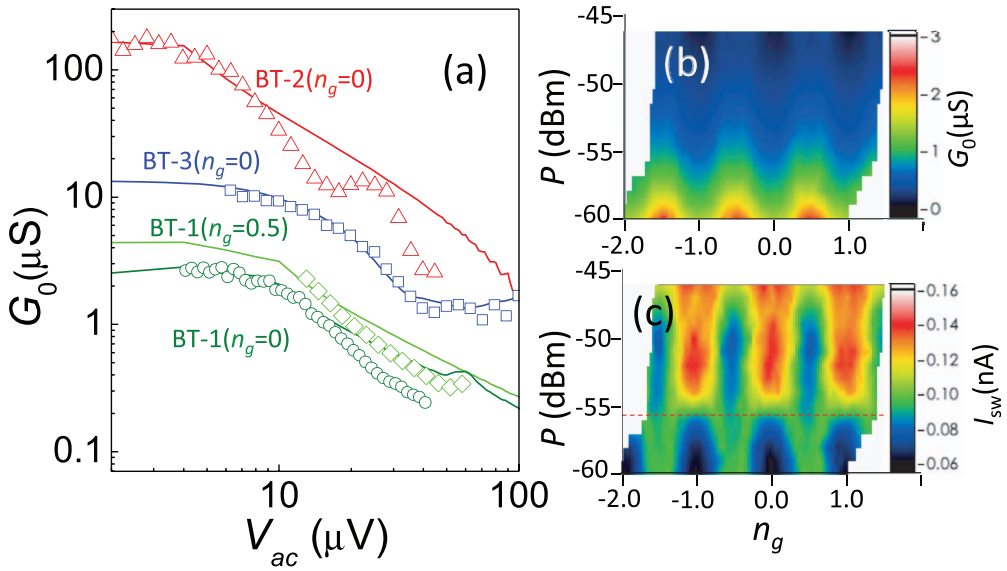

FIG. 4. (a) The zero-bias conductance, G_0 as a function of RF amplitude, which has been converted to V_{ac} as described in text. The symbols mark the experimental data while the curves are predictions of phase diffusion model. The RF frequencies used were 2.14 GHz, 1.6 GHz and 0.227 GHz for BT-1, 2 and 3 respectively. Because of a larger influence in a resonant circuit, V_{ac} for BT-3 is scaled by a factor of 3. (b) Intensity plot of zero-bias conductance G_0 of BT-1 as a function of V_g and P_{ac} of 2.14 GHz excitation. (c) Intensity plot of switching current, I_{sw} of BT-1. On the contrary, the Coulomb oscillation for I_{sw} becomes inverted when $P_{ac} > -55$ dBm. We note that the drift of gate charge has been removed in the above plots.

voltage. By gradually elevating the RF power, we observed that the onset voltage of the switching, V_{sw} and switching current both got higher and higher. In particular, V_{sw} increases linearly with RF amplitude as depicted in Fig. 3(d). In Fig. 3(b), one can see that at a low power, Eq. (2) explains the experiment data fairly well, but at a high power, the theory have a larger deviation, especially the switching current was under-estimated. For BT-2, which having robust phase coherency, the model better depicts the *IV* curves with RF excitation. The fitting parameter V_{ac} in Fig. 3(b) and 3(c) followed a linear dependence with the RF amplitude, $\sqrt{P_{ac}}$, indicating the phase diffusion model for θ is applicable to our BTs. Fig. 4(a) shows a summary of 3 BTs that how G_0 decays with RF amplitude, which is converted to V_{ac} by using the slope of V_{ac} (or V_{sw}) vs. $\sqrt{P_{ac}}$ curves as shown in Fig. 3(d). Because the large E_J/E_C values of BT-2 and BT-3, they did not show much difference when varying n_g. The data agree well with the curves calculated by using the phase diffusion model; though some deviations occur in BT-1, which displays stronger charging effect.

To understand how the charging effect influences the phase diffusion, we study the zero-bias conductance G_0 and switching current I_{sw} when varying n_g. As mentioned before, G_0 and I_{sw} respectively relate to the diffusion on phase θ and ϕ. The Coulomb oscillation in I_{sw} shown in Fig. 4(c) clearly gets inverted, while that of G_0 (Fig. 4(b)) does not. The above findings infer that the charge degree of freedom should be considered as a correction to Eq. (2), which based on a constant switching current as RF power increases. A successful correction should explain the inversion of Coulomb oscillation in I_{sw} so a model describing ac driving of central-island variable ϕ (or n) becomes the focal point.

IV. DISCUSSIONS ON RESULTS

A. Charge coupling model: two-level approximation

To work out this, we start from a much simple case, modeling the transistor as a spin system with two states, $|0\rangle$ and $|1\rangle$. This is plausible near the energy degenerate point for charge states $n_g \simeq 0.5$. By noting that $\varepsilon = 2E_C(1-2n_g)$, $\Delta = E_J \cos(\theta/2)/2 \simeq E_J/2$ and the Pauli operators

$\sigma_z = |0\rangle\langle 0| - |1\rangle\langle 1|$ and $\sigma_x = |0\rangle\langle 1| + |1\rangle\langle 0|$, we may re-write the transistor hamiltonian,

$$H_S = \varepsilon\sigma_z + \Delta\sigma_x.$$

The eigenstates are $|+\rangle = \cos\frac{\alpha}{2}|0\rangle + \sin\frac{\alpha}{2}|1\rangle$ and $|-\rangle = -\sin\frac{\alpha}{2}|0\rangle + \cos\frac{\alpha}{2}|1\rangle$, respectively corresponding to eigen energies of $\lambda = \sqrt{\varepsilon^2 + \Delta^2}$ and $-\sqrt{\varepsilon^2 + \Delta^2}$ with azimuthal angle $\alpha = \tan^{-1}(\Delta/\varepsilon)$.

There are two possible ways to introduce the ac-driving: σ_z and σ_x-coupling. As illustrate schematically in Fig. 4(c) and 1(d), because of the linear shape of our BTs, the ac voltages across the two consisting junctions are likely in phase so as to cancel out the direct influence on ϕ. Therefore the ac driving is more likely coupled to the BT through its quantum conjugate variable, n. We also note that if considering the electric dipole interaction due to excess charges on the island, one would prefer the σ_z-coupling as proposed in Jaynes and Cummings hamiltonian.[25] Assuming a time-dependent perturbation, $V = \gamma(t)\sigma_z = 4\eta E_C \cos\omega t$ and noting the wave function in interaction picture as $|\psi\rangle$, one may write down the differential equations for coefficients $c_\pm = \langle\pm|\psi\rangle$,

$$\begin{aligned} i\hbar\frac{d}{dt}\begin{pmatrix} c_+ \\ c_- \end{pmatrix} &= \begin{pmatrix} \langle +|\,V\,|+\rangle & e^{-i2\lambda t/\hbar}\langle +|\,V\,|-\rangle \\ e^{i2\lambda t/\hbar}\langle -|\,V\,|+\rangle & \langle -|\,V\,|-\rangle \end{pmatrix}\begin{pmatrix} c_+ \\ c_- \end{pmatrix} \\ &= \gamma(t)\begin{pmatrix} \cos\alpha & -e^{i2\lambda t/\hbar}\sin\alpha \\ -e^{-i2\lambda t/\hbar}\sin\alpha & -\cos\alpha \end{pmatrix}\begin{pmatrix} c_+ \\ c_- \end{pmatrix}. \end{aligned}$$

The solutions to above equations do not have close forms if $\gamma(t)$ is a sinusoidal function. Nevertheless, we can find approximation results if considering $\gamma(t)$ as a slow-varying function in respect to the dynamical phase factor $e^{i2\lambda t/\hbar}$. Using a similar approach for solving Rabi oscillation and discarding time derivative of $\gamma(t)$, one has

$$\frac{d^2c_0}{dt^2} + i2\frac{\lambda}{\hbar}\frac{dc_0}{dt} + \frac{\gamma}{\hbar}\left(\frac{\gamma}{\hbar} + 2\frac{\lambda}{\hbar}\cos\alpha\right)c_0 = 0$$

$$\frac{d^2c_1}{dt^2} - i2\frac{\lambda}{\hbar}\frac{dc_1}{dt} + \frac{\gamma}{\hbar}\left(\frac{\gamma}{\hbar} + 2\frac{\lambda}{\hbar}\cos\alpha\right)c_1 = 0.$$

In intermediate time scale, $\hbar\lambda^{-1} \ll t \ll \omega^{-1}$, $\gamma(t)$ can be viewed as a constant of time so as to yield the solution of $c_0 = Ae^{i\Omega_{0,+}t} + Be^{i\Omega_{0,-}t}$ and $c_1 = Ce^{i\Omega_{1,+}t} + De^{i\Omega_{1,-}t}$. Here the characteristic frequencies obey $\hbar\Omega_{0,\pm} = -\lambda \mp \sqrt{\lambda^2 + \gamma(\gamma + 2\lambda\cos\alpha)}$ and $\hbar\Omega_{1,\pm} = \lambda \pm \sqrt{\lambda^2 + \gamma(\gamma + 2\lambda\cos\alpha)}$. If the driving is small $\gamma \ll 2\lambda$ and far from resonance $\hbar\omega \ll 2\lambda$, the state would be mainly in ground state, allowing one to arbitrary choose an initial state $c_0(0) \simeq 1$ and $c_1(0) \simeq 0$. The solution becomes $c_1(t) \simeq -\gamma(t)\sin\alpha(e^{i\Omega_{1,0}t} - e^{i\Omega_{1,1}t})/2\lambda$, giving a probability in the excited state

$$P_1(t) = |c_1(t)|^2 \simeq \frac{\gamma^2(t)\sin^2\alpha}{2\lambda^2}\left[1 - \cos\left(\Omega_{1,+} - \Omega_{1,-}\right)t\right] \simeq \frac{\gamma^2(t)\sin^2\alpha}{2\lambda^2}\left(1 - \cos\frac{2\lambda t}{\hbar}\right). \tag{3}$$

When t increases to $t \simeq \omega^{-1}$, the above approximation is broken down. Nevertheless, the decoherence time, t_2 and relaxation time, t_1 of the system set natural cutoffs for the validity of Eq. (3), making the dynamics Markovian when $t > t_1, t_2$. Namely, c_0 and c_1 are likely be "reset" under decoherence and relation processes, an assumption similar to the Drude model for electron conduction. We expect t_1 and t_2 would not exceed the inverse of driving frequency $t = \omega^{-1}$. When seeking a long time average of the excited state probability, we first average fast oscillations, namely the $\cos(2\lambda t/\hbar)$ term to get $\langle P_1\rangle_{\text{fast}} \simeq \gamma^2(t)\sin^2\alpha/2\lambda^2$, followed by averaging the slow varying part in $\gamma(t)$ to obtain $\langle P_1\rangle_{\text{slow}} \simeq \langle\gamma^2(t)\rangle\sin^2\alpha/2\lambda^2$. By putting all parameters using E_C and E_J, one gets

$$\langle\cos\phi\rangle = \langle\sigma_z\rangle = (\langle P_0\rangle - \langle P_1\rangle)\sin\alpha = \left(1 - 8\eta^2\sin^4\alpha\frac{E_C^2}{E_J^2}\right)\sin\alpha. \tag{4}$$

Fig. 5(a) shows the calculated results of various driving amplitude η. One can clear see an inversion of Coulomb oscillation when $2\sqrt{2}\eta E_C/E_J \simeq 1$.

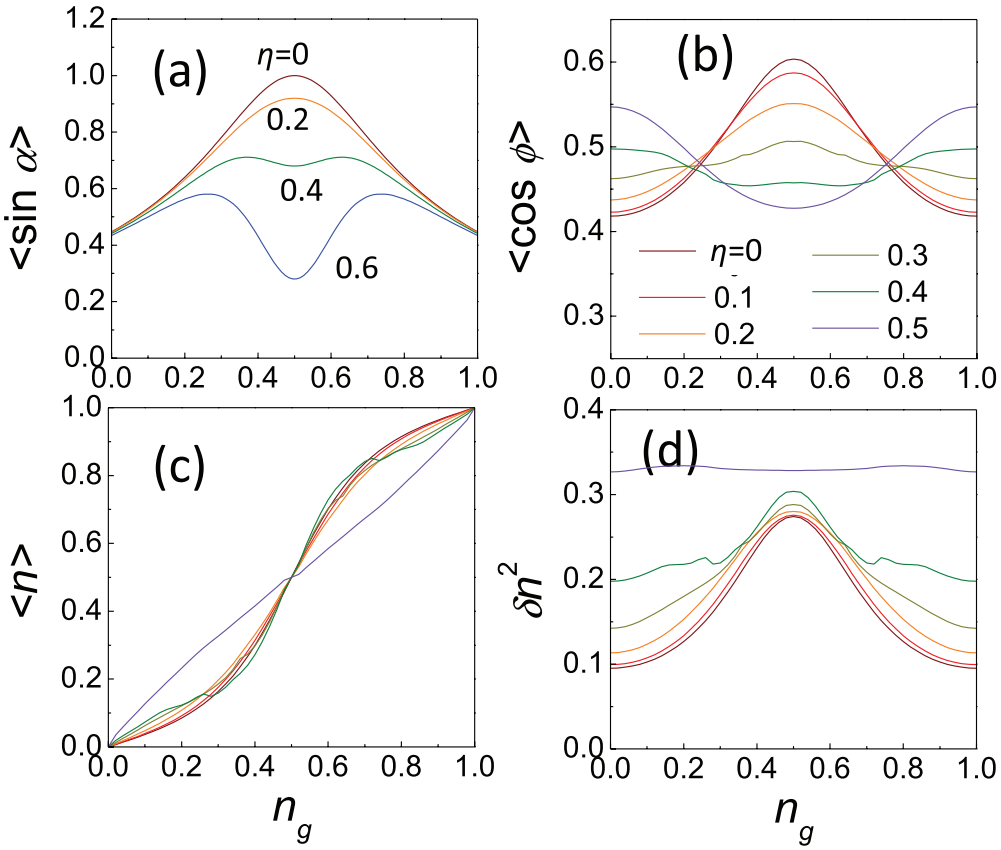

FIG. 5. (a) Calculated $\langle \sin\alpha \rangle$ by using 2-level approximation. (b) The calculation result of $\langle \cos\phi \rangle$as a function of n_g using Bloch wave calculation. Both results show the inversion of Coulomb oscillation at sufficient large driving amplitude around $\eta = 0.3$. (c) Average CP number $\langle n \rangle$ and (d) CP number fluctuation $\delta n^2 = \langle n^2 \rangle - \langle n \rangle^2$as a function of n_g at various η values. Up to $\eta = 0.4$, the charge diffusion is weak, and is majorly increases the CP number fluctuation at n_g is integers. At $\eta = 0.5$, the charge diffusion is pronounced to convert $\langle n \rangle$ vs. n_g curve a step-like curve into a straight line and the CP number fluctuation becomes a constant of n_g.

B. Charge diffusion: Floquet analysis of charge states

The spin system is an approximation, so we want to restore the hamiltonian introduced in the beginning with a perturbation reflecting the σ_z-coupling mentioned in the last section,

$$H = 4E_C(n - n_g)^2 + E_J \cos\phi + 4\eta E_C(n - n_g)\cos\omega t. \tag{5}$$

One can interpret the perturbation as an effective ac gate charge introduced by electromagnetic excitations, generating a general force $4\eta E_C \cos\omega t$ on CP number, n-n_g. The solutions should obey Floquet's theorem that $\Psi(t) = e^{-i\varepsilon t/\hbar}\sum_n c_n(t)|n\rangle$, where $c_n(t)$ are periodic function of t that can be expanded by Fourier series, $c_n(t) = \sum_m c_{n,m}e^{-im\omega t}$. Therefore each coefficient $c_{n,m}$ would follow eigen-equations:

$$\left[4E_C\left(n-n_g\right)^2 - m\hbar\omega\right]c_{n,m} + \frac{E_J}{2}\left(c_{n-1,m}+c_{n+1,m}\right) + 4\eta E_C\left(n-n_g\right)\left(c_{n,m+1}+c_{n,m-1}\right) = \varepsilon c_{n,m}.$$

By truncating high energy charge states (large $|n - n_g|$) and high frequency components (large $|m|$), one can solve this eigenvalue problem, and found corresponding eigenfunctions.

The ac driving produced band-like energy spectrum, which can be labeled by quantum numbers s and r, in which s denotes the band index, corresponding to the eigenstates of the un-excited problem while r is related to the average order m in Fourier series. Each pure state has an average energy

$E \simeq \varepsilon + \langle s, r|m|s, r\rangle \hbar\omega$. We may calculate the following expectation value for each pure state,

$$\langle s, r| \cos\phi \, |s, r\rangle = \sum_{n,m} c^*_{n,m} c_{n+1,m} + \sum_{n,m} c^*_{n,m} c_{n-1,m}.$$

We propose that experimentally the stationary state is not a pure state, but a mixing state in the space spanned by the low energy states in a low energy window $E - E_{\min} \leq k_B T$, in which $E_{\min}$ denotes the lowest average energy of the pure states. The ensemble average can be determined by a density matrix ρ, $\langle \cos\phi \rangle = \mathrm{tr}(\rho \cos\phi)$. With an assumption of random phase approximation and thermal equilibrium distribution, one can discard off-diagonal elements in ρ and assign Boltzmann factors in diagonal elements to obtain,

$$\langle \cos\phi \rangle = \frac{\sum_{r,s} e^{-(E-E_{\min})/k_B T} \, \langle s, r| \cos\phi \, |s, r\rangle}{\sum_{r,s} e^{-(E-E_{\min})/k_B T}}. \tag{6}$$

In Fig. 5(b) we present the calculated result with $E_J = 2E_C$, $\hbar\omega = 0.1E_C$, $k_B T = 0.1E_C$ for various η values from 0 to 0.5. Again we obtained an inversion of Coulomb oscillation.

We also calculated average CP number $\langle n \rangle$ and charge fluctuation $\delta n^2 = \langle n^2 \rangle - \langle n \rangle^2$ as illustrated in Fig. 5(c) and 5(d). At a low η values, the charge number as a function of n_g shows a step-like curve but the step structure gradually gets smoothed out as the η value increases. Especially when η is 0.5, the curve evolves into a straight line, featuring a complete smeared off of single charge property by strong charge diffusion. Correspondingly, the charge fluctuation is maximal at $n_g = 0.5$ at a low η value, but becomes almost flat when $\eta = 0.5$. Similar to the summational phase-diffusion model, the charge diffusion can be intuitively predicted from the phase-charge duality in the BTs.

The charge diffusion model leads to more interesting consequences worthy of future studying. First, one can directly probe n by using a charge sensor to confirm the enhanced charge diffusion. Second, the coupling depends on the polarization of the excitation electromagnetic wave. By changing the polarization of the wave, one should tune the system from phase diffusion to charge diffusion. Because of the interplay of θ and n in a BT, we expect that certain interesting phenomena arise if one separately tunes the ac driving of θ and n. For example, it may lead to the highly accurate charge pumping as reported in Ref. 15. We leave these topics for future studies.

V. CONCLUSIONS

In summary, we have experimentally measured the dc response of Bloch transistors under RF/MW excitations. Through the current-voltage characteristics, we observed pronounced superconducting phase diffusion. The phase diffusion, which can be quantified by the zero-bias resistance, ${G_0}^{-1}$ increases as RF/MW power increases. On the other hand, RF/MW-induced charge diffusion can be deduced from the switching current as a function of gate voltage. The charge diffusion can be analyzed using an electric dipolar interaction between the photon field and excess charge on the central island. A duality in phase and charge can be applied to understand the charge diffusion phenomenon.

ACKNOWLEDGMENTS

The authors acknowledge the assistance in RF/MW measurement from Y. W. Suen at NCHU and SET fabrications from J. C. Wu and C. S. Wu at NCUE. We also have fruitful discussions with C. D. Chen and J. C. Chen. This work was financially supported by National Science Council of Taiwan through grant No. NSC99-2112-M-005-007-MY3 and Center of Nanoscience and Nanotechnology, NCHU.

[1] D. Averin and K. Likharev, in *Mesoscopic Phenomena in Solids* (Elsevier Science Publishers, Amsterdam, 1991), pp. 173–271.
[2] D. J. Flees, S. Han, and J. E. Lukens, Phys. Rev. Lett. **78**(25), 4817–4820 (1997).
[3] L. S. Kuzmin and D. B. Haviland, Phys. Rev. Lett. **67**(20), 2890 (1991).

[4] M. Devoret, D. Esteve, H. Grabert, G. Ingold, H. Pothier, and C. Urbina, Phys. Rev. Lett. **64**(15), 1824–1827 (1990).
[5] S. M. Girvin, L. I. Glazman, M. Jonson, D. R. Penn, and M. D. Stiles, Phys. Rev. Lett. **64**(26), 3183–3186 (1990).
[6] J. B. Kycia, J. Chen, R. Therrien, á. Kurdak, K. L. Campman, A. C. Gossard, and J. Clarke, Phys. Rev. Lett. **87**(1), 017002 (2001).
[7] G. Schon and A. Zaikin, Physics Reports **198**, 237–412 (1990).
[8] W. Guichard and F. W. J. Hekking, Phys. Rev. B **81**(6), 064508 (2010).
[9] W. Danchi, F. Habbal, and M. Tinkham, Appl. Phys. Lett. **41**(9), 883–885 (1982).
[10] Y. Koval, M. Fistul, and A. Ustinov, Phys. Rev. Lett. **93**(8), 087004 (2004).
[11] S. Corlevi, W. Guichard, F. W. J. Hekking, and D. B. Haviland, Phys. Rev. Lett. **97**(9), 096802 (2006).
[12] T. M. Eiles and J. M. Martinis, Phys. Rev. B **50**(1), 627 (1994).
[13] S. Liou, W. Kuo, Y. Suen, W. Hsieh, C. Wu, and C. Chen, Chinese Journal of Physics **45**, 230 (2007).
[14] J. P. Pekola, J. J. Toppari, M. Aunola, M. T. Savolainen, and D. V. Averin, Phys. Rev. B **60**(14), R9931–R9934 (1999).
[15] A. O. Niskanen, J. P. Pekola, and H. Seppä, Phys. Rev. Lett. **91** (17), 177003 (2003).
[16] R. Schoelkopf, P. Wahlgren, A. Kozhevnikov, P. Delsing, and D. Prober, Science **280**(5367), 1238 (1998).
[17] T. Buehler, D. Reilly, R. Brenner, A. Hamilton, A. Dzurak, and R. Clark, Appl. Phys. Lett. **82**, 577 (2003).
[18] W. Kuo, C. S. Wu, J. H. Shyu, and C. D. Chen, Phys. Rev. B **75**(1), 014517–014516 (2007).
[19] Y. Nakamura, Y. A. Pashkin, and J. S. Tsai, Nature **398**(6730), 786–788 (1999).
[20] T. M. Eiles and J. M. Martinis, Phys. Rev. B **50**(1), 627–630 (1994).
[21] P. Joyez, P. Lafarge, A. Filipe, D. Esteve, and M. H. Devoret, Phys. Rev. Lett. **72**(15), 2458–2461 (1994).
[22] M. Matters, W. J. Elion, and J. E. Mooij, Phys. Rev. Lett. **75**(4), 721–724 (1995).
[23] S. Liou, W.-C. Chien, and W. Kuo, AIP Advances **2**(3), 032161–032113 (2012).
[24] S. Liou, W. Kuo, Y. W. Suen, C. S. Wu, and C. D. Chen, New Journal of Physics **10**(7), 073025 (2008).
[25] E. T. Jaynes and F. W. Cummings, Proceedings of the IEEE **51**(1), 89–109 (1963).